AFRL-SR-BL-TR-98-0471

REPORT DOCUMENTATION PAGE

Form Approved
OMB No. 074-0188

1. AGENCY USE ONLY (Leave blank)	2. REPORT DATE	3. REPORT TYPE AND DATES COVERED
	5-11-98	Final Technical Report 11/15/96-2/15/98

4. TITLE AND SUBTITLE

"Whole-Field Measurements in Gas-Phase Turbulent Flows"

5. FUNDING NUMBERS

F49620-94-1-0283

6. AUTHOR(S)

Dr. Paul Dimotakis

7. PERFORMING ORGANIZATION NAME(S) AND ADDRESS(ES)

Dr. Paul Dimotakis
Department of Aeronautics
MC 301-46
California Institute of Technology
Pasadena, CA 91125

8. PERFORMING ORGANIZATION REPORT NUMBER

9. SPONSORING / MONITORING AGENCY NAME(S) AND ADDRESS(ES)

AFOSR/NA
110 Duncan Ave., Room B115
Bolling AFB, DC 20332-8080

10. SPONSORING / MONITORING AGENCY REPORT NUMBER

F49620-94-1-0283

11. SUPPLEMENTARY NOTES

12a. DISTRIBUTION / AVAILABILITY STATEMENT

Approved for public release;
distribution unlimited.

19980602 078

STRIBUTION CODE

13. ABSTRACT *(Maximum 200 Words)*

Aerooptical phenomena associated with the propagation of optical beams and imaging through turbulent index-of-refraction fields have been investigated. Using simultaneous imaging of optical-beam distortion and the turbulent index-or-refraction field, we have documented near-field behavior, following propagation through moderate-to-high Reynolds number jets and shear layers. For both flows, propagation through turbulence may result in the formation of caustics. Preliminary measurements using the Palomar 200" telescope confirm the formation of caustics in atmospheric propagation, using bright stars as sources. Spatial wavefront and wavefront-tilt measurements of beams emerging from jet and shear-layer regions exhibit non-Kolmogorov behavior. Preliminary efforts to reconstruct images through turbulence indicate the need for both amplitude and wavefront-tilt measurements for reliable image reconstruction.

14. SUBJECT TERMS

DTIC QUALITY INSPECTED 4

15. NUMBER OF PAGES

24

16. PRICE CODE

17. SECURITY CLASSIFICATION OF REPORT	18. SECURITY CLASSIFICATION OF THIS PAGE	19. SECURITY CLASSIFICATION OF ABSTRACT	20. LIMITATION OF ABSTRACT
Unclassified	Unclassified	Unclassified	UL

GRADUATE AERONAUTICAL LABORATORIES
CALIFORNIA INSTITUTE of TECHNOLOGY
Pasadena, California 91125

Whole-field measurements of turbulent flow for the study of aero-optical effects

Paul E. Dimotakis

Air Force Office of Scientific Research
Grant No. F49620-94-1-0283

Final Technical Report: Period ending 14 February 1998

14 April 1998

Summary/Overview

The purpose of this effort was to investigate the behavior of three-dimensional scalar fields in fully-developed, gas-phase, turbulent flows; to further our understanding of phenomena that rely on the behavior of scalar gradients, such as aerooptical effects, imaging through a turbulent medium, such as the atmosphere; as well as laser propagation through, and scattering by, gas-phase turbulent flows. It has been a collaborative effort with the Physics and Astronomy departments at Caltech, and the Jet Propulsion Laboratory, and comprised of several experimental and theoretical/modeling parts that deal with scalar-fields and their aerooptical effects in various free-shear flows. It has benefited from equipment and instrumentation developed under cosponsorship by AFOSR Grant No. F49620–94–1–0353 and AFOSR/DURIP Grant No. F49620–95–1–0199. In this three-year effort, we have investigated the structure of index-of-refraction fields in high Reynolds number gas-phase turbulence, along with aerooptical phenomena associated with beam propagation through such fields. Flows specifically investigated include jets and shear layers. Out results have shed light on a host of phenomena that are important in the context of aerooptics that had not been previously addressed.

1. Introduction

The research program, "Whole-field measurements of turbulent flow for the study of aero-optical effects," completed under AFOSR support, Grant No. F49620–94–1–0283, was focused on the study and characterization of the multidimensional geometrical structure of scalar fields generated by fully-developed turbulence, with an emphasis on investigations of index-of-refraction fields as they pertain to aerooptical phenomena and the needs of aerooptical applications.

Aerooptical phenomena involve the propagation of transmitted beams, such as lasers, imaging beams, as occur in ground-based astronomical and other observations, observations of the earth from space, as well as from rapidly-moving air-borne platforms. In the course of this propagation, wavefront coherence of the transmitted/received optical beam is distorted by index-of-refraction fluctuations in the intervening turbulent medium, often compromising its utility.

In these phenomena, the resulting wavefront degradation may loosely be regarded as the consequence of two interaction regimes. These are the result of small-amplitude, relatively-long time-scale distortions, accumulated over long propagation distances, as occurs in propagation through the atmosphere (Tatarskii 1961, Clifford 1978, Roddier 1981, Goodman 1985), and from relatively-higher-amplitude, possibly short-time phase distortions, a consequence of near-field turbulence near the receiving/transmitting end, depending on its characteristics (ground-based, airborne, *etc.*). Implemented and contemplated means to address such distortions depend on the characteristics of each type, or combination, of these effects. Long-range atmospheric wavefront distortion, resulting in the scintillation of stars in ground-based telescopes, for example, is characterized by order-millisecond time scales. These permit the employment of "rubber-mirror" adaptive-optics techniques in a feedback-control-loop for substantial real-time wavefront phase-error corrections (Babcock 1953, 1990, Tyson 1991).

Near-field effects, as would be produced in traversing through boundary layers or shear layers can be characterized by time scales that are too short to permit "rubber-mirror" adaptive-optics techniques. By way of example, a boundary layer with a thickness of $\delta_{\rm bl} \approx 1\,{\rm cm}$, generated on the exterior of an optical window on an airplane moving at $U_\infty \approx 250\,{\rm m/s}$, would be characterized by a frequency spectrum scaled by a characteristic large-scale boundary-layer time of,

$$t_{\rm bl} = \frac{\delta_{\rm bl}}{U_\infty} \simeq 4 \times 10^{-5}\,{\rm s}\ . \tag{1a}$$

Separated shear layers from the same airplane would tend to be thicker, say, $\delta_{\rm sl} \approx 10 - 50\,{\rm cm}$, with accordingly-longer characteristic times, *i.e.*,

$$t_{\rm sl} \;=\; \frac{\delta_{\rm sl}}{U_\infty} \;\simeq\; 4 \times 10^{-4} - 2 \times 10^{-3}\ {\rm s}\ . \tag{1b}$$

At the high Reynolds numbers that would apply in these scenarios, however, the frequency-content of index-of-refraction fluctuation spectra is very large. The index-of-refraction fluctuation time scales extend to several orders of magnitude lower, corresponding to very high frequencies, albeit at lower amplitudes. For such aerooptical interactions, possible mitigation techniques include nonlinear, phase-conjugation wave-mixing optical methods, flow control to alter the index-of-refraction fields to ones characterized by lower distortions, or to ones hopefully lending themselves to easier optical correction/adaptation.

In all these applications, progress is hampered by an incomplete knowledge of the geometrical structure of the index-of-refraction field in the turbulent flow, through which the optical beam must propagate. Successes to date, using "rubber-mirror" optics, for example, rest more with the general power of closed-loop control methods, rather than a good model for the system being controlled; the effects of the intervening turbulent medium, in this case.

The purpose of the work undertaken under sponsorship of this AFOSR Grant and described below, initially under Dr. J. McMichael and completed under Prof. M. Glauser as program managers, has been to investigate the structure of scalar fields in turbulent flows and index-of-refraction fields, in particular, and its relation to aerooptical phenomena.

2. Progress, accomplishments, and new findings

2.1 Near-field aerooptical effects

Weak aerooptical effects, corresponding to optical-beam propagation through a confined turbulent region, can be described in terms of the wavefront-propagation phase function,

$$\varphi \;=\; \int_{\Omega} \mathbf{k}(\mathbf{x},t)\cdot \mathrm{d}\mathbf{x} \;, \tag{2a}$$

for each beam (ray) that emerges from the turbulence-containing domain, Ω. In this expression,

$$\mathbf{k} \;=\; \frac{2\pi}{\lambda}\,\hat{\mathbf{k}} \;, \tag{2b}$$

is the local wavevector of the beam, with λ the local value of the wavelength, as it is altered (*e.g.*, eikonal equation) in direction, $\hat{\mathbf{k}}$, and magnitude, $2\pi/\lambda$, by the fluctuating index-of-refraction field, $n(\mathbf{x},t)$.

For small deflections, we may neglect the change in the propagation direction, say, along the x-axis, and approximate this integral, expressed in terms of the transverse coordinate, say, y, at any one time, t, *i.e.*,

$$\varphi(y) \;=\; k_0 \int_{\Omega} n(x,y)\,\mathrm{d}x \;, \tag{2c}$$

where $k_0 = 2\pi/\lambda_0$, is the wavevector magnitude (in vacuum).

If the index of refraction fluctuations are scaled by Δn, *e.g.*, if they arise as the result of mixing of two fluids with an index of refraction n_1 and n_2, corresponding, for example, to the indices of refraction of two freestream fluids entrained in a turbulent shear-layer region, then we'll have a maximum index-of-refraction excursion of $\Delta n = |n_1 - n_2|$. If Δn is not too large, the leading-order beam-propagation effect may be regarded as the phase-accumulation in the original x-direction of propagation, say, as a function of a transverse coordinate, y. This will be scaled by the index-of-refraction magnitude, Δn, and the extent of the turbulent region, L, in the direction of propagation. This motivates the definition of a scaled propagation perturbation phase function,

$$\tilde{\varphi}(y) \;\equiv\; \frac{\varphi(y)}{k_0\,L\,\Delta n} \;\simeq\; \frac{1}{\Delta n}\int \left[\,n(x,y) - n_\infty\,\right]\mathrm{d}\left(\frac{x}{L}\right) \;, \tag{3}$$

which can be used to characterize weak aerooptical effects in confined, fluctuating index-of-refraction turbulent regions. This will be used to illustrate some of the aeroptical effects and in the proposed studies of near-field interactions.

Wavefront functions from turbulent regions are typically estimated in the laboratory using direct-measurement techniques, such as Shack-Hartmann lenslet arrays, shearing interferometers, *etc.* Quantitative imaging techniques, however, permit a direct measurement of the instantaneous index-of-refraction field in a plane, *i.e.*, $n(x, y)$, as required in Eq. 3, allowing a numerical computation of the scaled phasefront-propagation function, to a high accuracy and resolution.

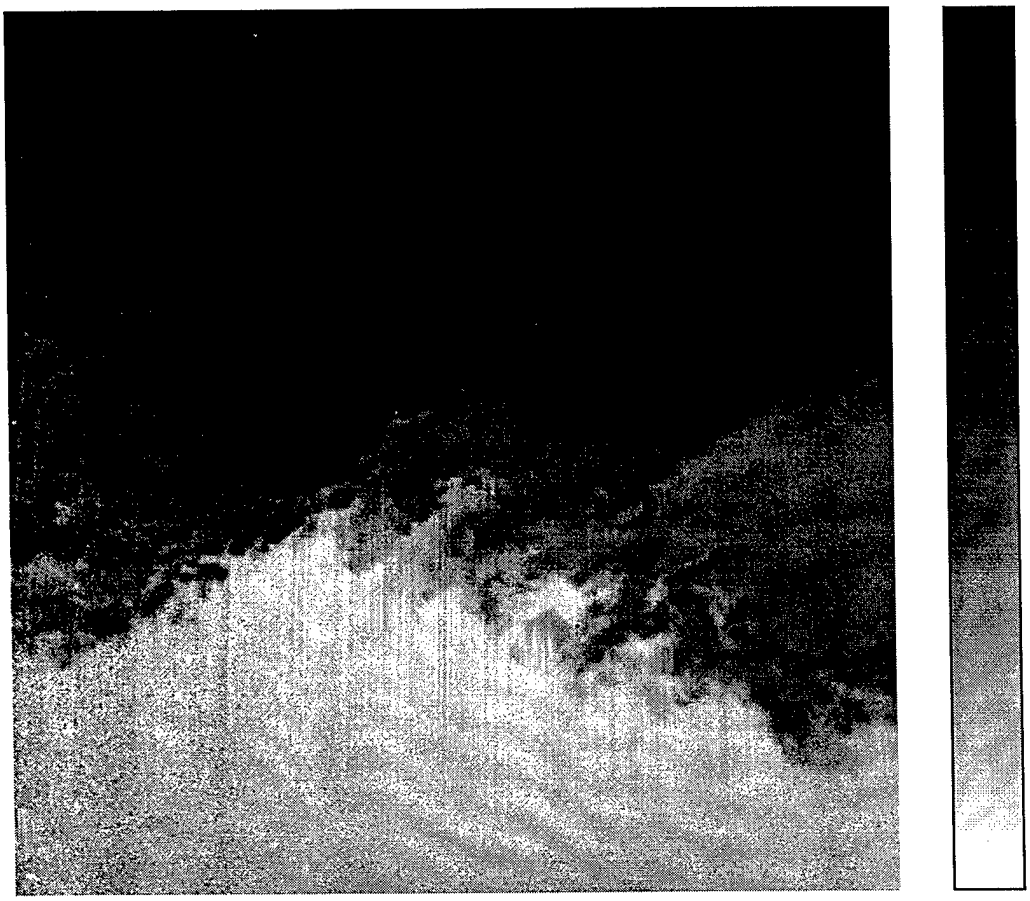

FIG. 1 Rayleigh-scattering image slice in the mid-span plane of a low-compressibility ($M_c = 0.15$), high Reynolds number ($Re \simeq 2 \times 10^5$), shear-layer. Gray scale (right) denotes index of refraction. Note mixed-fluid regions of near-uniform index of refraction.

The results of sample calculations, performed on data recorded previously (under support of this grant) in subsonic (low-compressibility) shear layers (convective Mach number, $M_c \simeq 0.15$), as well as supersonic shear layers with moderate ($M_c \simeq 0.54$) and high ($M_c \simeq 0.96$) compressibility, will be shown below (Fourguette *et al.* 1998). An example of such data is included here as Fig. 1. Exploiting the fact that aerooptical deflections of rays are small, in this case, these data were image-processed to remove the streaks caused by the aerooptical interaction, to estimate the variable index-of-refraction field. The remaining small-scale streaks in Fig. 1 are a manifestation of the no-deflection approximation. As noted above, the index of refraction difference in this flow was generated through the use of nitrogen and ethylene as the freestream gases.

The normalized phase integral integration (Eq. 3) was carried across the imaged field of view, with $L \approx 2\delta$ (*i.e.*, roughly, twice the local shear-layer width) equal to the extent of the imaged field, and $n_\infty = n_1$ the (low) index of refraction of the high-speed fluid. Figure 2 depicts the scaled phase function, $\tilde{\varphi}(y/L)$, for the data in Fig. 1, reproduced here to provide a direct visual comparison.

It is clear from the scalar-field image data and the resulting phase integral calculations that the large-scale-structure organization of the flow produces locally positive- and negative-lens effects. In particular, depending on the distance between the turbulent region and the aperture of the receiving optics, the effective positive lenses may produce caustics along the way, as was found in high-pressure experiments of turbulent jets using the same gases (Fourguette, Dimotakis, % Ching 1995).

Also shown are ensemble-averaged spatial spectra of the normalized phase-front-tilt integrals,

$$\psi(y/L) \;=\; \frac{1}{L}\,\frac{\partial\tilde{\varphi}}{\partial y} \;=\; \frac{1}{L\,\Delta n}\int \frac{\partial n}{\partial y}\,\mathrm{d}\left(\frac{x}{L}\right) \;, \tag{4a}$$

i.e.,

$$S_\psi(\kappa_y\,L) \;=\; \mathcal{FT}\{\,<\,\psi(y'/L)\,\psi[(y-y')/L]\,>_{y'}\,\}\;. \tag{4b}$$

These are plotted in Fig. 3, with lines of increasing solidity indicating increasing compressibility. The phase-front-tilt spectra can be seen to be nearly white over much of the resolved spatial wavenumber range. Interestingly, compressibility has a stronger effect at the high wavenumber end of the spectrum, with an influence that is non-monotonic with increasing M_c. In particular, the lowest scalar gradients

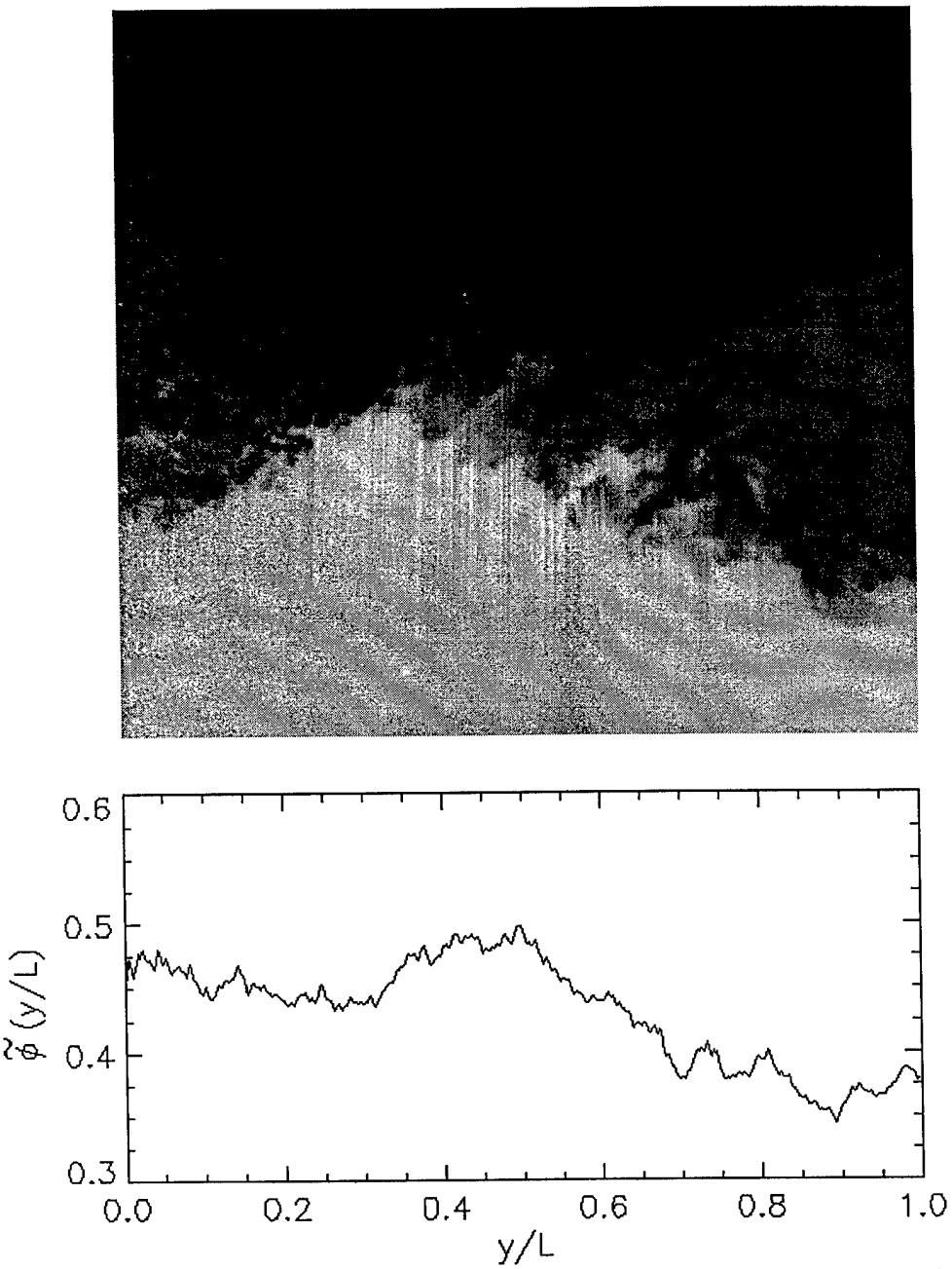

FIG. 2 Subsonic shear-layer scalar-field image and normalized phase integral, $\tilde{\varphi}(y)$, Eq. 3, for a high-Re, subsonic, shear-layer realization (same data as in Fig. 1).

(smallest phase-front tilts) are encountered at the moderate (intermediate) compressibility case. This is probably attributable to a combination of Mach-number and Reynolds-number effects, which do not act in the same way. Similar behavior has been observed in direct measurements of molecular mixing in chemically-reacting shear layers.*

* Work on mixing presently in progress, sponsored by AFOSR Grant No. F49620–98–1–0052.

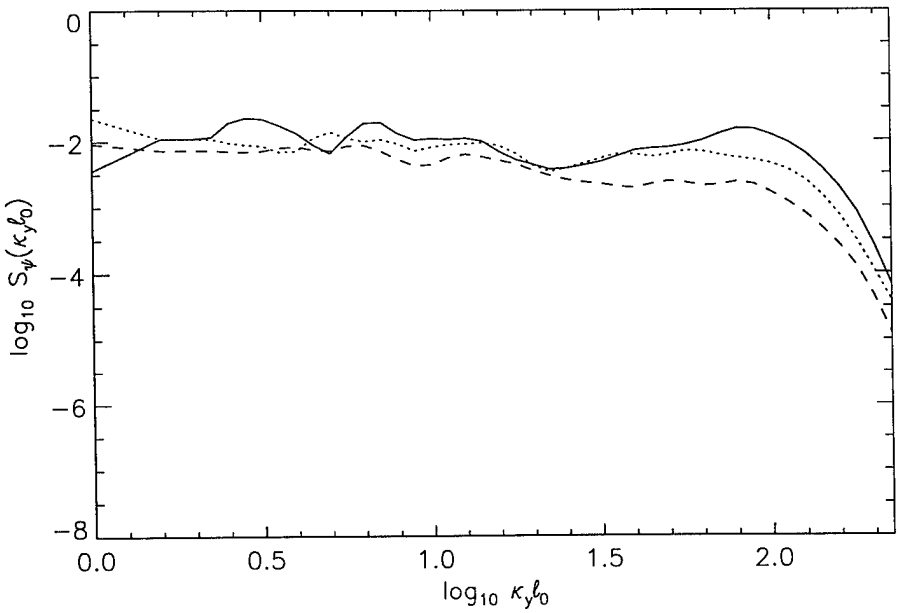

FIG. 3 Ensemble-averaged spectra of phase-front-tilts for shear layers of increasing compressibility. Lines of increasing solidity correspond to convective Mach numbers of $M_c = 0.15$, 0.54, and 0.96.

Similar calculations were also performed on turbulent-jet data, more-recently acquired in the GALCIT Variable-Pressure Combustion Facility (VPCF), under support of this grant. Pressure in this facility can be varied, $0.1\,\text{atm} \leq p \leq 15\,\text{atm}$, permitting Reynolds numbers to be varied over a large range. More importantly, however, optical signals can be enhanced by operating at elevated pressures. Examples from preliminary experiments at $p = 4\,\text{atm}$ and $p = 10\,\text{atm}$ will be shown below. These also rely on Rayleigh scattering, utilizing ethylene as the jet fluid, discharging in a quiescent reservoir of nitrogen.

The $Re \simeq 3.0 \times 10^4$ jet data at $p = 10\,\text{atm}$ were recorded previously (Fourguette *et al.* 1995), with new data at the lower Reynolds number as part of a more-recent investigation.** Examples are shown in Fig. 4 and record a slice of the scalar field and associated aerooptical distortion for a beam (laser sheet) propagating from left to right, in a plane containing the jet axis. The earlier ($p = 10\,\text{atm}$) experiments relied on a cryogenically-cooled (1024 × 1024)-pixel CCD camera (Photometrics, Model 200 series). The elevated ambient pressures resulted in higher index-of-refraction gradients and signal-to-noise ratios.

** Jet Reynolds numbers here are cited using the ambient, reservoir-fluid (N_2) viscosity.

FIG. 4 Examples of Rayleigh-scattering images of gas-phase turbulent jets (C_2H_4 injected into N_2), for $Re \simeq 1.5 \times 10^4$, at $p \approx 4\,\text{atm}$, $1.4 \lesssim x/d_{\text{jet}} \lesssim 7.5$ (left), and $Re \simeq 3.0 \times 10^4$, at $p \approx 10\,\text{atm}$, $1.5 \lesssim x/d_{\text{jet}} \lesssim 6.5$ (right). Aerooptical effects due to index-of-refraction variations are evident in these images.

The more recent experiments relied on a back-illuminated, higher-quantum-efficiency (ca. 75%) cryogenically-cooled (low-noise) CCD camera (Princeton Instruments, Model TKB1024-1), permitting images to be acquired at a (lower) ambient-tank pressure of $p \approx 4\,\text{atm}$.

As with the shear-layer experiments, the primary interest in this part of the proposed effort is to investigate the geometry of the scalar field and the associated distortions of optical wavefronts. Note that, in these experiments, the fluid Schmidt number is $Sc \approx 1$ (*cf.* $Sc \approx 2.0 \times 10^3$ for the liquid-phase jets – Catrakis & Dimotakis 1996). The higher molecular diffusivity in the gas phase produces a smoother scalar field and lower scalar gradients (at small scales). In comparison with liquid-phase data, such experiments can be used to quantify Sc and Re effects on the scalar field.

Before an analysis of scalar level sets or beam propagation can be made, the aerooptical "streaks" evident in Fig. 4 must be removed, as was necessary for the shear-layer data described above (Fig. 1). We have developed a new technique, based on complex Fourier filtering, which attempts to remove these streaks by application of a notch-type filter to the Fourier-transformed images, followed by a subsequent inverse-Fourier transformation. An example of the results of this procedure is shown

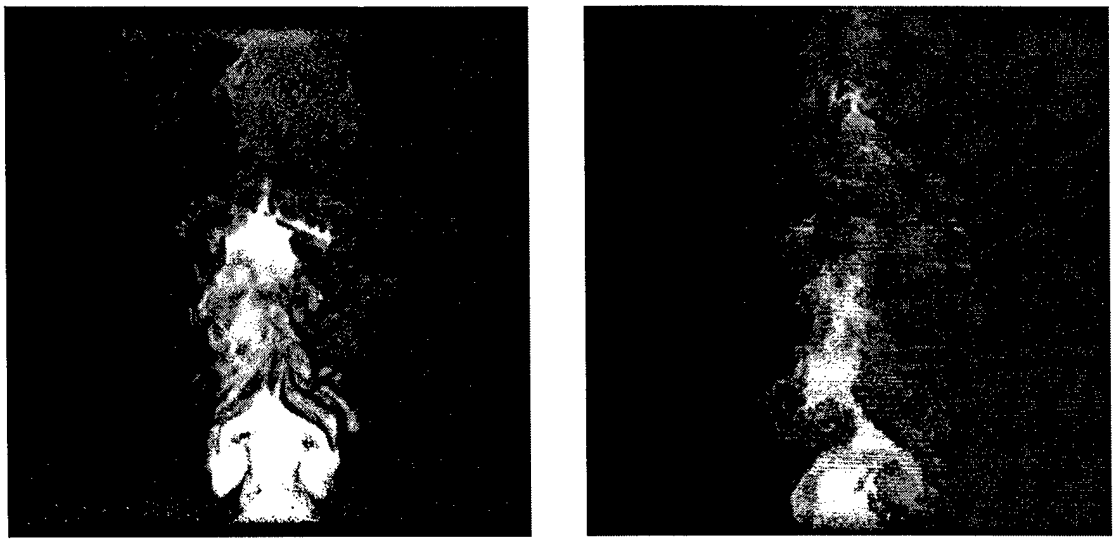

FIG. 5 Examples of Fourier filtering applied to images of gas-phase turbulent jets at $Re \simeq 1.5 \times 10^4$ and $p \simeq 4\,\mathrm{atm}$ (left), and $Re \simeq 3.0 \times 10^4$ and $p \simeq 10\,\mathrm{atm}$ (right), to remove aero-optical "streaks" (*cf.* Fig. 4).

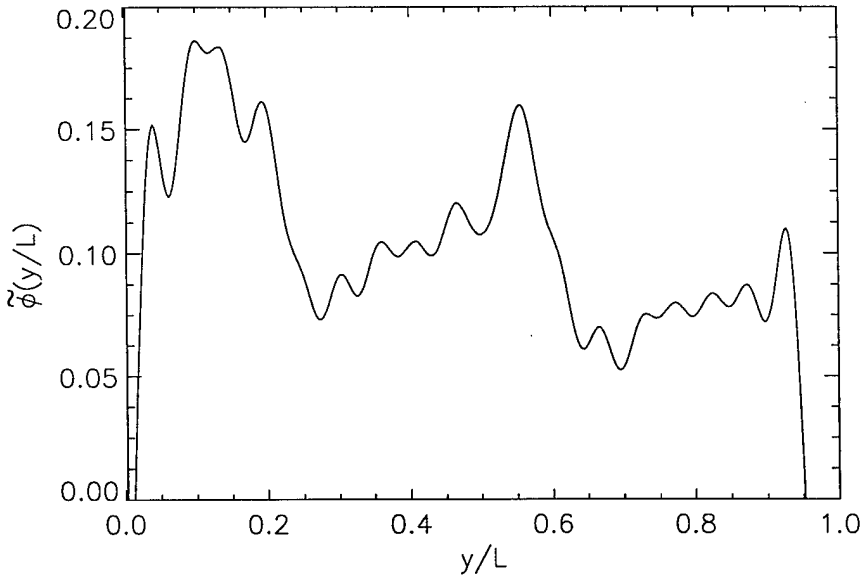

FIG. 6 Normalized phase-propagation integral computed from a single, Fourier-filtered image of a $Re \simeq 1.5 \times 10^4$, $p \simeq 4\,\mathrm{atm}$ gas-phase turbulent jet.

in Fig. 5. While there are ways to further improve the filtering process, the simple notch-type filter used to remove the streaks in Fig. 5 can be seen to be effective.

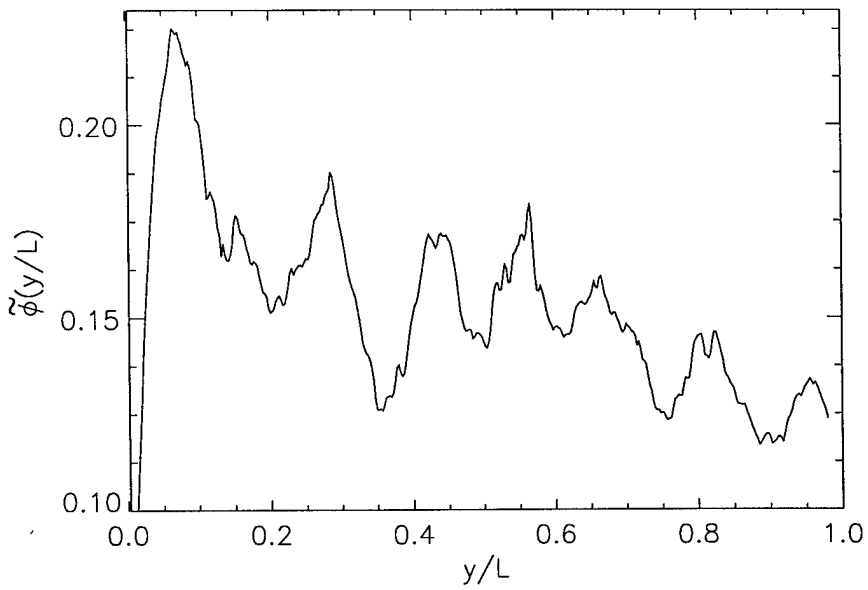

FIG. 7 Normalized phase-propagation integral computed from a single, Fourier-filtered image of a $Re \simeq 3.0 \times 10^4$, $p \simeq 10\,\mathrm{atm}$ gas-phase turbulent jet.

Using the Fourier-filtered images, similar phase-propagation integrals can be computed, as before (Eq. 3). Examples of such calculations, derived from the data in the Fourier-filtered turbulent-jet images, are shown in Figs. 6 and 7. For these calculations, n_∞ is the index of refraction of the ambient (reservoir) fluid (N_2, in this case) and $\Delta n = n_{\mathrm{jet}} - n_\infty$ (*cf.* Eq. 3).

Phase-front-tilt spectra (Eq. 4) can also be computed for these data. They are shown in Fig. 8 for the two Fourier-filtered images depicted in Fig. 5. Both *Re* and pressure effects can be expected to be reflected in this statistic.

Experiments over a range of Reynolds numbers, with several realizations for each flow condition, will allow an investigation of *Re* effects on the scalar fields and the resulting beam-propagation characteristics, as well as an isoscalar-surface analysis utilizing the framework described above, that was applied previously to liquid-phase turbulent jets (Catrakis & Dimotakis 1996).

The work comprised of the aerooptical calculations and the new gas-phase turbulent-jet experiments described above were performed in collaboration with H. Catrakis, as a continuation of work begun with D. Fourguette, as part of the recently-completed investigations, under this grant. A more complete discussion of these results is beyond the purposes of this proposal. A first report of this work will

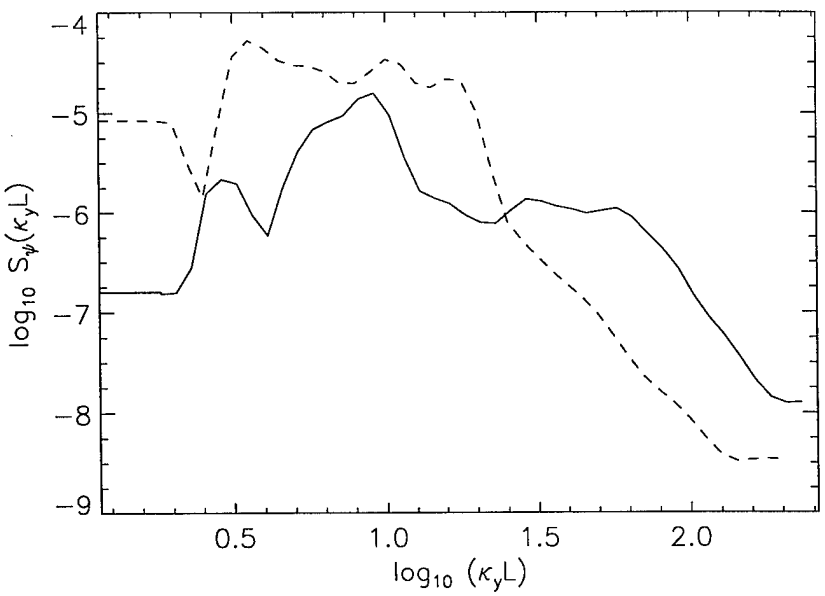

FIG. 8 Phase-front-tilt spectra for ethylene/nitrogen turbulent jets. Dashed line: $Re \simeq 1.5 \times 10^4$ and $p \simeq 4\,\mathrm{atm}$. Solid line: $Re \simeq 3.0 \times 10^4$ and $p \simeq 10\,\mathrm{atm}$.

be presented in the upcoming AIAA Fluid Dynamics meeting (Dimotakis, Catrakis, & Fourguette 1998).

2.2 Long-range optical-beam propagation in the atmosphere

Using ground-based astronomical observatories provides a useful test bed for optical beam/imaging terrestrial applications from space-borne platforms. While imaging from airborne platforms is easier, in that the optical sweep caused by the high speeds of orbiting satellites and other objects do not have to be contended with, nevertheless, both applications must contend with the turbulent atmosphere. In both cases, as with long-range optical propagation within the atmosphere, an important issue is the formation of caustics. Caustics are singularities that represent a many-to-one-to-many transformation in the propagation. When coupled with finite signal-to-noise ratios, adaptive-optics systems have a scant chance recovering beam energy that has gone through a caustic.

Examples of images of Arcturus, used as a bright point-source reference, acquired with the 200″ Palomar telescope, with the Cassini-CCD (1024^2) camera system described above, is depicted in Fig. 9. These were binned in (2×2)-pixel regions in real time and read at 20 frames/s (at a 512×512 pixel resolution).

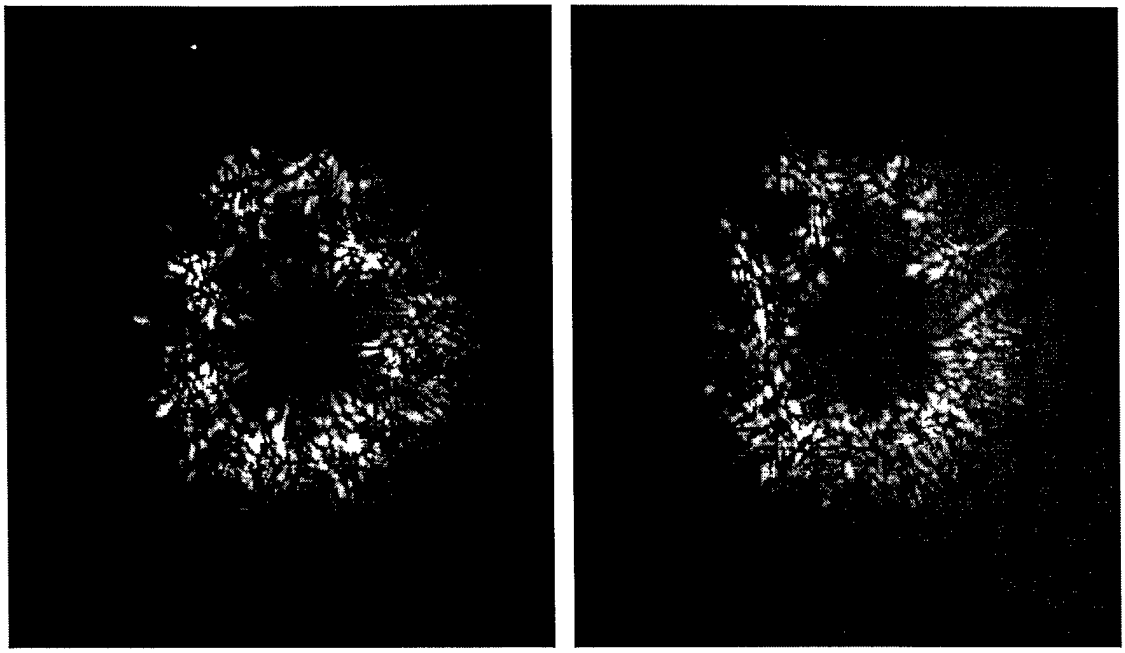

FIG. 9 Two out-of-focus images of Arcturus, recorded in good-to-moderate seeing conditions, to illustrate caustic formation, on the Palomar 200″ telescope, 50 ms apart, cropped to 11 × 12.8 arc-sec (275 × 320 binned pixels) each.

Figure 9 depicts two images from this sequence (50 ms apart), formed of a bright star (Arcturus) in the first hours of the night (good-to-moderate seeing), purposely out of focus, to investigate the tendency of caustic formation by the turbulent atmosphere. The magnification of the optical system was, roughly, 50 (unbinned) pixels/arc-sec. The hexagonal support structure of the 200″ reflector can be discerned imprinted on the pattern of caustics. Substantial differences in caustic patterns can be seen to have occurred in the intervening 50 ms that are attributable to the unsteady, turbulent atmosphere.

This effort, which began under this grant, was suspended because it soon became clear that imaging limitations imposed by our Cassini-CCD-based system prevented us from addressing atmospheric scintillation phenomena. These occur on time scales in the range of $10^{-3}\,\mathrm{s} \lesssim t \lesssim 10^{-2}\,\mathrm{s}$, or so. We are hoping we will have the opportunity to resume it, following the completion of our high framing-rate digital-imaging system, presently under development under a DURIP Grant No. F49620–95–1–0199, "High speed/resolution/dynamic-range imaging system for subsonic and supersonic turbulent flows," and continuing under AFOSR Grant No. F49620–98–1–0052, "Mixing, chemical reactions, and combustion in sub-

sonic and supersonic turbulent flows," and NSF Grant No. AST9618880, "Ex-Post Facto Diffraction-Limited Imaging Through Atmospheric Turbulence."

2.3 Controlled-turbulence aerooptics investigations

In an exploratory effort to develop a system for accurate image reconstruction from turbulence-degraded images, we have considered approaches that record wavefront aberrations, along with the resulting image. In these preliminary efforts, wavefront aberrations were estimated using a single, out-of-focus image. Intensity variations in an out-of-focus image correspond to variations in wavefront curvature at the entrance pupil.[12] In laboratory experiments, we have explored the limitations of making a single out-of-focus measurement, as well as a simultaneous in-focus measurement.

Variations in wavefront curvature will cause light from different parts of the pupil to come to a focus at different places along the optical axis. If ℓ is the distance between the resulting focal position, as determined by the local wavefront curvature, and the nominal focal plane, we have,

$$\ell = \frac{f^2}{2\,k}\,\nabla^2\varphi \ , \tag{5}$$

where φ is the wavefront phase function (Eq. 2), f is the focal length of the imaging system, and k is the wavenumber. Note that $\ell = \ell(x,y)$ is a local variable, as defined over the pupil aperture-interior coordinates. If the detector is displaced a distance $\ell_{\rm det}$ from the nominal focal plane, then,

$$\frac{\ell}{\ell_{\rm det}} = \frac{1-(I_0/I)^{1/2}}{1-(I_0/I)^{1/2}\,\ell_{\rm det}/f} \approx \frac{I-I_0}{2\,I_0} \ , \tag{6}$$

where $I = I(x,y)$ is the intensity field in the out-of-focus image and $I_0 = I_0(x,y)$ is the intensity field in the absence of phase aberrations. The approximation is valid for $\Delta I/I_0 = (I-I_0)/I_0 \ll 1$ and $\ell_{\rm det}/f \ll 1$. These equations are based on purely geometric arguments, and are valid as long as diffractive effects are negligible, *i.e.*, provided $\ell_{\rm det}^2 \gg < \ell^2 >$.

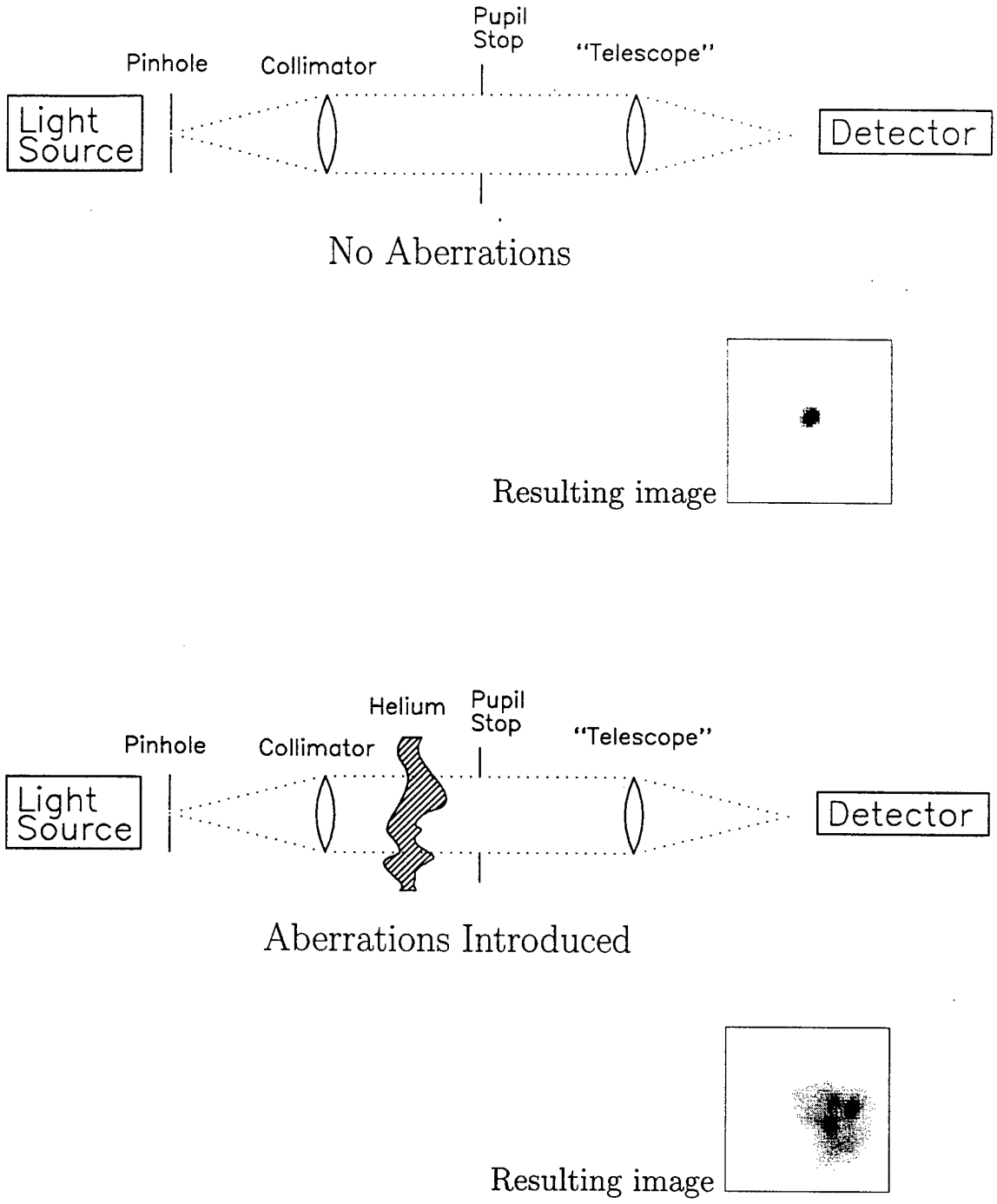

FIG. 10 Helium-jet turbulent-flow aberrator setup. Actual images in each case.

To transform a map of out-of-focus intensity measurements, $I(x, y)$, into wavefront curvature, $\nabla^2\varphi$, we need to know $I_0(x, y)$, the intensity field in the absence of phase aberrations. The simplest assumption is that (the mapped) $I_0(x, y)$ is uniform across the pupil or, in other words, that there are no amplitude fluctuations.

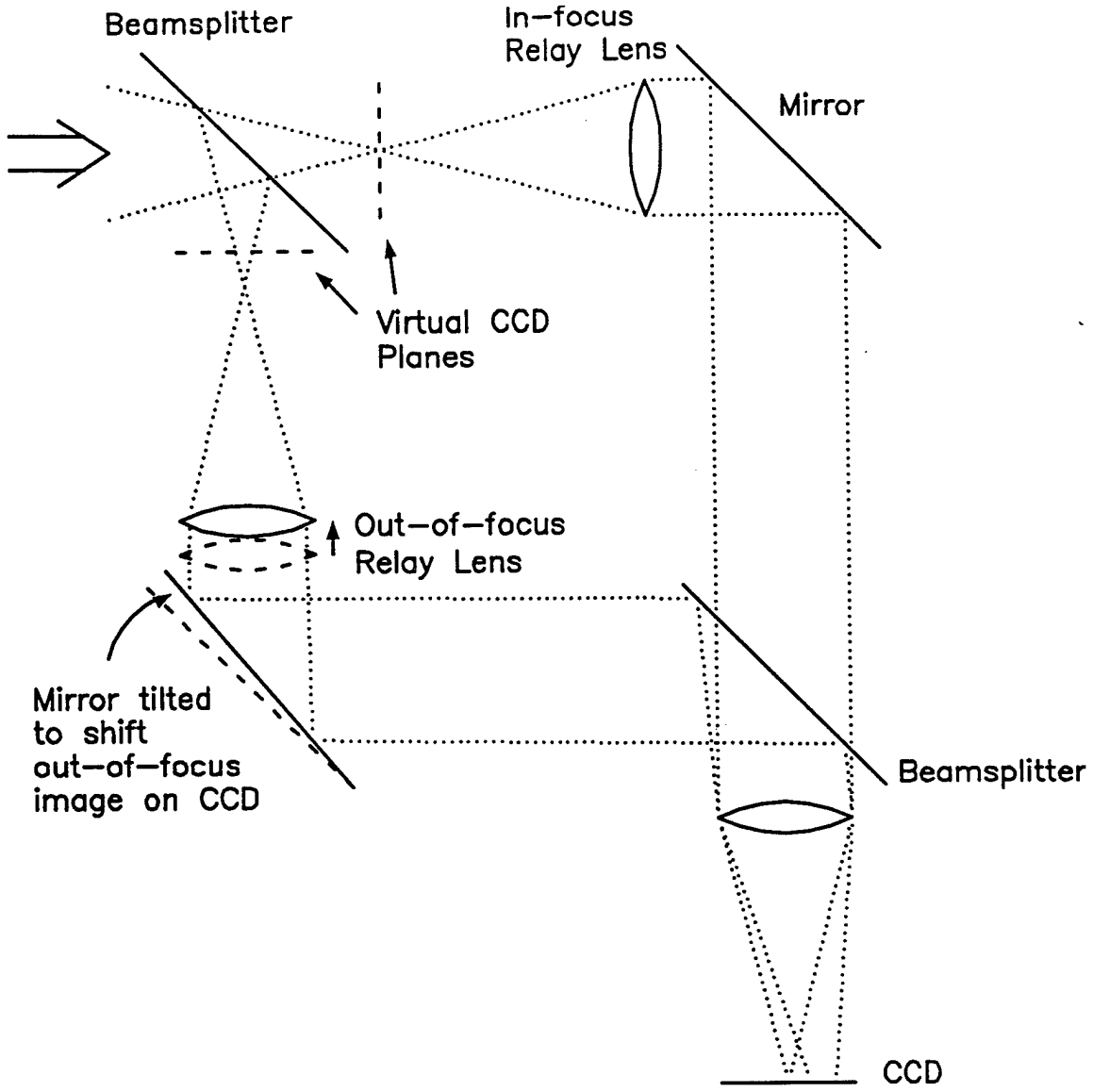

FIG. 11 Simultaneous in- and out-of-focus imaging system optics.

Note that static amplitude variations (such as spatial variations in the transmission of the optical system or in detector sensitivity) do not affect these measurements, since only the ratio I/I_0 appears in these equations. In practice, then, to account for static amplitude variations, I_0 can be taken to be constant in time, with spatial variations determined by examining the intensity with no aberrations present.

Equation 5, relating ℓ to $\nabla^2\varphi$, is for a monochromatic source. In our preliminary experiments, a white-light source was used. If we assume that the phase and amplitude fluctuations are achromatic, from a single image we can determine φ for

all wavelengths, by applying the equations above at every value of k desired.

The relationship between $\nabla^2\varphi$ and φ was estimated by nearest-neighbor differencing, *i.e.*,

$$\nabla^2\varphi_{i,j} \simeq \varphi_{i-1,j} + \varphi_{i+1,j} + \varphi_{i,j-1} + \varphi_{i,j+1} - 4\varphi_{i,j} \ . \tag{7}$$

Assuming there are N points where $\nabla^2\varphi$ is sampled, this yields N linear equations with N variables. Absent additional information, the transformation from φ to $\nabla^2\varphi$ is not strictly invertible.† This can be seen by noting that $\varphi_{i,j} = c$ (piston term) for all (i,j) gives $\nabla^2\varphi = 0$ for any value of c. Such a piston-term contribution is irrelevant, however, in the reconstruction.

To establish a transformation from $\nabla^2\varphi$ to φ, a singular-value decomposition of the transformation matrix from φ to $\nabla^2\varphi$ was performed, which allowed a "least-squares" inversion. Given the geometry of the problem, *i.e.*, how the out-of-focus image is sampled, a single inverse transformation was used for every realization of the data.

Once the phase is known across the pupil, the scalar electric field, $E = A\,e^{i\varphi}$, with A assumed constant, can be treated by Fresnel diffraction instead of geometrical optics. To determine the scalar electric field at the out-of-focus plane of observation, we use the Kirchhoff scalar diffraction equation with Neumann boundary conditions (Ref. 13, p. 431),

$$E(x,y,z) = \frac{k}{2\pi i}\int\limits_{\mathcal{P}} e^{ikR}\left(1 + \frac{i}{kR}\right)\frac{z}{R^2}\,E(x',y',0)\,\mathrm{d}x'\,\mathrm{d}y' \ , \tag{8}$$

where $R = \sqrt{(x-x')^2 + (y-y')^2 + z^2}$, and $\mathcal{P}$ is the area of the pupil. This calculation must be performed separately for every value of k. Knowing the system throughput at different wavelengths, the intensity at each wavelength can be combined to give the expected broadband image. The out-of-focus image expected from these phase aberrations can then be compared to the out-of-focus image received. The difference between the expected and received images can, in principle, be put through the same process as the original out-of-focus image, to derive an improved estimate of φ at the pupil. The process can be further iterated until the pupil phase distribution, when Fresnel-diffracted to the out-of-focus plane of observation, matches the observed out-of-focus image.

---

† Boundary information, for example, would allow an inversion of this relation.

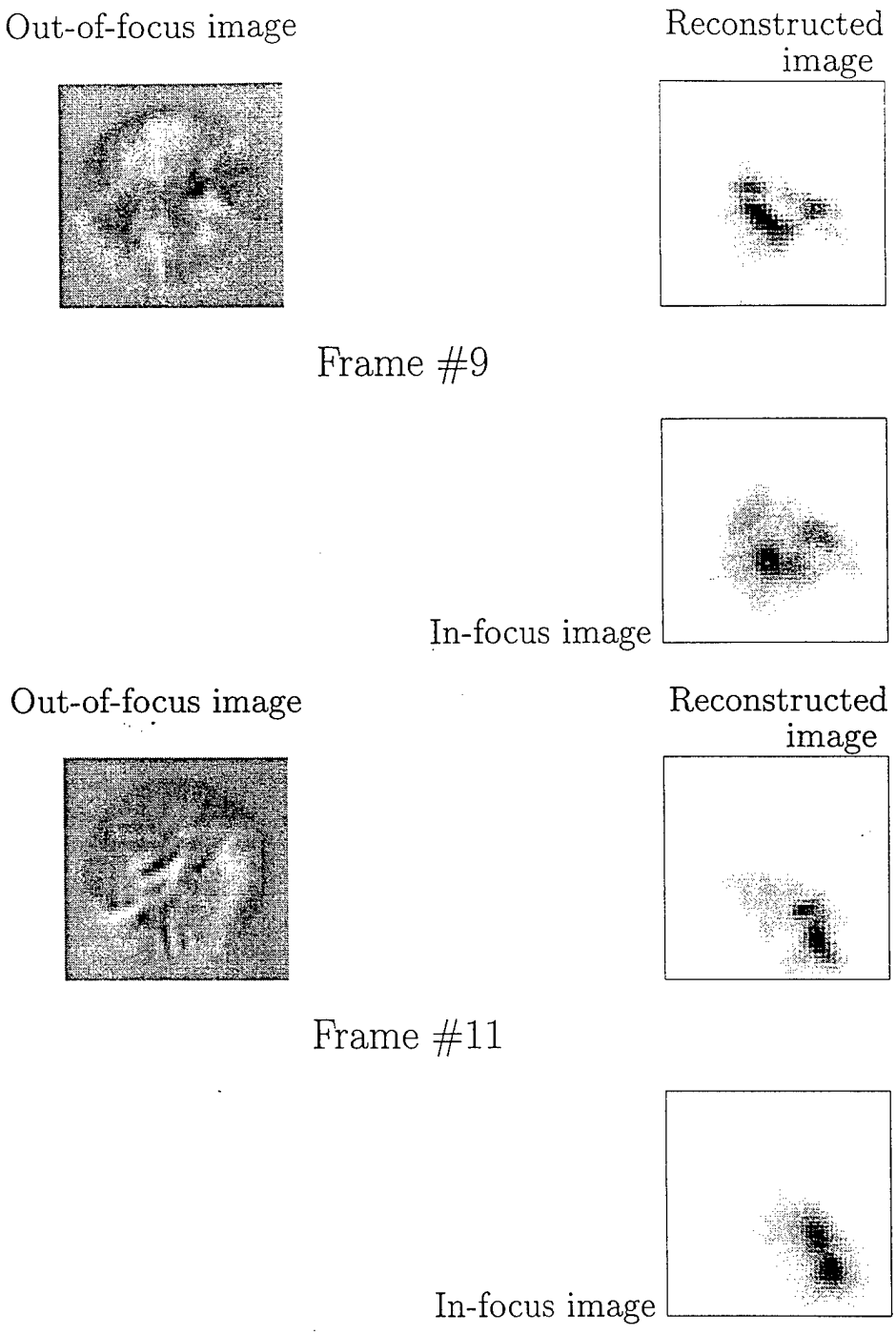

FIG. 12 Out-of focus (left), reconstructed and actual in-focus images (right), for two frames (top/bottom).

This procedure was explored in a bench-top setup by imaging a lit pinhole with and without turbulent-flow aberrations. To add turbulent-flow aberrations, the collimated light beam from the point light source was passed through the flow

of a turbulent downward-directed helium jet in air (Fig. 10). The resulting in- and out-of-focus images were recorded on our Cassini camera, using an optical scheme that split the single CCD plane accordingly (Fig. 11). Sample data from two double-image frames extracted from a single sequence are depicted in Fig. 12. The figure includes the out-of-focus image (left), the reconstructed in-focus image using the scheme outlined above (top right), and the actual in-focus image recorded (bottom right). As can be seen, the two are in qualitative agreement.

The electric field in the pupil plane is related to the electric field in the focal plane by Fraunhofer diffraction, which is equivalent to a Fourier transform. This means that a Point Spread Function (PSF) can be determined from the phase aberrations. With the appropriate PSF in hand, an in-focus image can be deconvolved to remove the effects of the turbulent distortions. In our case, we should be able to deconvolve the in-focus images to yield the point source that is found in the absence of aberrations. Pursuing this route, we find, however, that our PSF does not match the actual in-focus image recorded within any reasonable errors. The disagreement between the estimated PSF and the measured in-focus image implies that a systematic error has been made in the computations.

Some amplitude fluctuations are expected when observing astronomical objects. At $\lambda \simeq 0.7\,\mu$m, the atmospheric transfer function due to amplitude variations reaches a value of ~ 0.9.[14] Assuming that all of the intensity variations seen are due to phase fluctuations, the latter will be overestimated. We also note that, roughly speaking, the transformation from $\nabla^2\varphi$ to φ in this geometry amplifies errors by a factor of ~ 8. Therefore, a modest amplitude fluctuations will produce relatively-large phase errors, and a correspondingly poor PSF estimation.

The preliminary investigations outlined above are the result of a collaborative effort with B. Kern and D. Lang.

3. References

BABCOCK, H. W. 1953 *Publ. Astron. Soc. Pac.* **65**.

BABCOCK, H. W. 1990 *Science* **249**, 253.

CATRAKIS, H. J. & DIMOTAKIS, P. E. 1996 "Mixing in turbulent jets: scalar measures and isosurface geometry," *J. Fluid Mech.* **317**, 369–406.

CLIFFORD, S. F. 1978 "The Classical Theory of Wave Propagation in a Turbulent Medium," in *Laser Beam Propagation in the Atmosphere* (J. W. Strohbehn, Ed., Springer-Verlag).

DIMOTAKIS, P. E., CATRAKIS, H. J. & FOURGUETTE, D. C. 1998 "Beam propagation and Phase-Front Integrals in High Reynolds Number Shear Layers and Jets," *AIAA* 29$^{\text{th}}$ *Plasmadynamics and Lasers Conference*, Paper 98–2833.

FOURGUETTE, D. C., DIMOTAKIS, P. E. & CHING, W.-K. 1995 "Whole-field index-of-refraction measurements in turbulent non-reacting jets," *AIAA* 26$^{\text{th}}$ *Plasmadynamics and Lasers Conference*, Paper 95–1980.

FOURGUETTE, D. C., SLESSOR, M. D., BOND, C. L. & DIMOTAKIS, P. E. 1998 "Planar-imaging and chemically-reacting investigations of incompressible and compressible, shear-layer flows," in preparation.

GOODMAN, J. W. 1985 *Statistical Optics* (Wiley).

JACKSON, J. D. 1975 *Classical Electrodynamics* (2^{nd} edition, Wiley, New York).

RODDIER, F. 1981 "The Effects of Atmospheric Turbulence in Optical Astronomy," in *Progress in Optics* **XIX** (E. Wolf, Ed., North-Holland).

RODDIER, F. 1988 "Curvature sensing and compensation: a new concept in adaptive optics," *Appl. Optics* **27**, 1223–1225.

RODDIER, F. & RODDIER, C. 1986 "Modeling atmospheric effects in adaptive optics systems for astronomical telescopes," *Proc. Soc. Photo-Opt. Instrum. Eng.* **628**, 298–304.

TATARSKII, V. I. 1961 *The effects of the turbulent atmosphere on wave propagation* (McGraw-Hill, New York).

TYSON, R. K. 1991 *Principles of adaptive optics* (Academic Press, Boston).

4. Personnel

4.1 Personnel supported by this Grant

- Catrakis, H. J., Assistant Scientist, Aeronautics.‡
- Chase, Stephen, Undergraduate Research Assistant (through June 1997).
- Dahl, E. E., Member of the Technical Staff, Aeronautics.
- Dimotakis, P. E., John K. Northrop Professor of Aeronautics & Professor of Applied Physics (PI).
- Fourguette, D. C., Senior Research Fellow, Aeronautics (through November 1996).♯
- Gornowicz, G. G., Graduate Research Assistant, Aeronautics (through March 1997).*
- Kern, B. D., Graduate Research Assistant, Astronomy, Caltech.
- Lang, D. B., Research Engineer, Aeronautics.
- Shan, J. W., Graduate Research Assistant, Aeronautics.
- Shekar, K., Undergraduate Research Assistant (through September 1997).

4.2 Other collaborators

- Collins, S. A., JPL (digital imaging).
- Elliot, T. S., JPL (digital imaging).
- Martin, C., Prof. Physics, Caltech.
- Wadsworth, M., JPL (digital imaging).

---

‡ Starting 1 July 1998, Assistant Professor, U. C. Irvine.

♯ Presently with Rice Systems, Inc.

* presently with DreamWorks, SKG.

5. Publications of work supported by this Grant

FOURGUETTE, D. C., DIMOTAKIS, P. E. & CHING, W.-K. 1995 "Whole-field index-of-refraction measurements in turbulent non-reacting jets," *AIAA* 26th *Plasmadynamics and Lasers Conference*, Paper 95–1980.

GORNOWICZ, G. G. 1997 *Continuous-field Image-Correlation Velocimetry and its Application to Unsteady Flow Over an Airfoil*, California Institute of Technology, Aeronautical Engineer's thesis.

DIMOTAKIS, P. E., CATRAKIS, H. J. & FOURGUETTE, D. C. 1998 "Beam propagation and Phase-Front Integrals in High Reynolds Number Shear Layers and Jets," *AIAA* 29th *Plasmadynamics and Lasers Conference*, Paper 98–2833, to appear.

FOURGUETTE, D. C., SLESSOR, M. D., BOND, C. L. & DIMOTAKIS, P. E. 1998 "Planar-imaging and chemically-reacting investigations of incompressible and compressible, shear-layer flows," in preparation.

6. Interactions/transitions

External interactions and collaborations with Air Force personnel during this period have included:

- Discussions on aerooptics, optical-beam propagation, and wavefront spectra with Dr. Demos Kyrazis, ABL Technology Division of Phillips Lab.
- Collaborations and discussions with Dr. Bruce Masson's group, Phillips Lab, at the time, on measurements of atmospheric temperature spectra from an airborne platform. Specifically, we assisted in the data analysis, built a pair of high frequency-response temperature sensors for them (used for flight measurements), and provided guidance and methodology to assess in-situ frequency-response characteristics for such spectral measurements.
- Discussions with YAL–1A Airborne Laser System Program Office at Kirtland AFB.

7. Honors/promotions/awards

Honors, degrees, promotions, and awards received during period, as well as, 'life-time achievement honors such as Nobel prize, honorary doctorates, and society fellowships prior to this effort', by personnel associated with this effort:

- Catrakis, H. J.:
  - Ph.D. degree, Aeronautics, California Institute of Technology (June 1996).
  - Appointed, Assistant Professor in Mechanical Engineering, U. C. Irvine, starting 1 July 1998.
- Dimotakis, P. E.:
  - John K. Northrop Chair, Aeronautics, Caltech (February 1995).
  - Associate Fellow, AIAA (June 1989).
  - Fellow, Am. Phys. Society (November 1980).
- Gornowicz, G. G.:
  - Aeronautical Engineer's Degree, California Institute of Technology (June 1997).